Diagnosis of Alzheimer's Disease Through Beta-Amyloid Detector

Group 5
Harleen Klair, Ariel Motsenyat, Isra Zahid,
Eman Chowdhury, Salim Lakhi
Health Solutions Design Projects II
IBEHS 2P03
April 12, 2021

Abstract

Alzheimer's disease (AD) is a progressive brain disorder that causes patients to experience cognitive impairment. It is difficult to definitively diagnose the disease as quantifiable symptoms can only be seen postmortem in procedures where a sample of the brain tissue is examined alongside clinical measures. Synthetic biology tools have been used to detect beta-amyloid and tau in the cerebrospinal fluid (CSF), which are biomarkers for AD. Due to this, our team designed a biological circuit that can be used as a diagnostic tool for AD that detects the presence of beta-amyloid and releases green fluorescent protein (GFP). Moreover, we modelled our circuit using Matlab SimBiology and ran simulations across various beta-amyloid levels found in the CSF. Through these simulations, we concluded that our biological circuit can be used to diagnose early stage AD. Finally, we proposed multiple wet-lab experiments to construct and test the efficacy of our biological circuit.

Introduction

Alzheimer's disease is an irreversible, progressive brain disorder that is more prevalent in individuals over the age of 65 [1]. Patients typically experience memory loss, language problems and cognitive impairment. AD usually develops slowly, making it difficult to recognize symptoms in the early stages. Currently, the only way to definitively diagnose a case of AD is through confirmation by autopsy [2]. Without this examination, patients can only be diagnosed with either a "possible case of Alzheimer's dementia" [3]. Early diagnosis of AD is crucial as it allows patients to begin treatment early and delay further cognitive impairment they will experience in the future [2].

Research suggests that in the early stages of AD, changes in beta-amyloid levels in the CSF can be observed [4], [5]. Beta-amyloid may accumulate over time into amyloid plaques in the brain, causing a lower concentration of it in the CSF, which is a primary biomarker for AD [6], [7].Our proposed circuit involves the detection of beta-amyloid levels in CSF using a fluorescence assay with E. coli as the host cell and GFP as the output. CSF samples will be extracted using a lumbar or cisternal puncture. This procedure will prevent the interaction between CSF and potentially dangerous external environments or organisms, reducing the overall constraints in the diagnosis of AD [8].

Materials and Methods

To simulate the wet-lab experiments, Simbiology was used through MATLAB. The transcription rate of the Cofilin-TEVp and the LilrB2-TEVp cleavage site_GAL4VP16 is modelled under the constant rate assumption. hEF1a constitutively promotes these molecules and so the assumption states $rate_{transcription} = k_{trsc}$, where k_{trsc} is the constant of transcription of the hEF1a promoter [9]. The mRNA translation for either protein is defined as $rate_{translation} = \frac{[translation\ efficiency]}{[average\ mRNA\ lifetime]}$, see Table 3 in Appendix B for values and units. The mRNA half lives of both the Cofilin-TEV protein and LilrB2-TEV protein cleavage site value (2 minutes) were used in the calculation of the average mRNA lifetime based on the equation $average\ mRNA\ life\ time = \frac{[mRNA\ half\ life]}{log2}$ [10]. The translation efficiency is assumed to be the same as that from Elowitz and Leibier's model due to the similarity in assumptions made and in the host used [10].

Cofilin-TEVp and the LilrB2-TEVp undergo a complexation reaction in order to release GAL4-VP16 which in turn establishes the production of GFP.

Once the complexation occurs, Beta-Amyloid then binds to the LilrB2 surface receptor, initiating GAL4-VP16 release. As this release is dependent on the concentration of Beta-Amyloid, its reaction rate is defined by the following: $rate_{GAL4VP16\ Release} = kf \times Complex$, where $kf = [k_{trsc\ of\ hEF1a}] \times ((\frac{[Beta\ Amyloid]}{K})^{\mu H} \div (1 + (\frac{[Beta\ Amyloid]}{K})^{H}))$, with $H = 1$ [11]. Note that Beta-Amyloid and GFP's degradation is characterized by protein degradation reactions. With Beta-Amyloid, $rate_{protein\ degradation} = kd_{prot} \times [protein]$, with $kd_{prot} = \frac{ln2}{[protein\ half\ life]}$ and the half life of Beta-Amyloid being 9 hours [12]. For GFP, it is specified with the equation $rate_{GFP\ degradation} = kd_{GFP\ loss} \times [protein]$, where the $kd_{GFP\ loss}$ value is defined by the equation $kd_{GFP\ loss} = \frac{ln2}{[GFP\ half\ life]}$, with the half life of GFP being 26 hours [13].

The transcription of GFP occurs under the UAS-GAL4 promoter which is positively induced by GAL4-VP16. The transcription rate for GFP can be stated to be $rate_{GFP\ transcription} = [k_{trsc\ of\ UAS-GAL4}] \times ((\frac{[GAL4VP16]}{K})^{\mu H} \div (1 + (\frac{[GAL4VP16]}{K})^{H}))$, with $H = 2$ [#]. The $k_{trsc\ of\ UAS-GAL4}$ is estimated to be 100 bases/second due to that being the value stated to be the maximum transcription of RNA polymerase [14]. Note that the units here are easily converted to nM/s through the known length of the UAS-GAL4 promoter. However, due to the continued presence of baseline levels of transcription, there is an additional rate to consider here, the baseline transcription rate $k0_{tr}$. The value of $k0_{tr}$ will be estimated using the tps_{repr}, the repressed promoter strength, using the equation $k0_{tr} = tps_{repr} \times 60$ [15].

Lastly, the formula $rate_{translation} = \frac{[translation\ efficiency]}{[average\ mRNA\ half\ life]}$ was used for the GFP translation with the half life of GFP mRNA estimated to be about 7 hours [16]. Although the value of the GFP mRNA half-life is that of GFP mRNA, it is assumed that its half-life is numerically similar to that of GFP mRNA from a lab.

Our group proposes multiple wet-lab experiments to construct and test the efficacy of our biological circuit.

First, all of the genes of interest, specifically, hEF1a, Cofilin-TEVp, LilrB2_TCS_GAL4VP16, UAS-GAL4, and GFP will not need to be isolated due to their prior isolation from the iGEM Registry of Standard Biological Parts, as seen in Tables 1 and 2 in Appendix A. However, the components that are no longer available on the iGEM registry of standard biological parts will be obtained from sites such as IDT [17].

Second, the genes of interest will be assembled into two different plasmids, as shown in Figure 1. For plasmid 1, the hEF1a, Cofilin-TEVp, and LilrB2_TCS_GAL4VP16 genes will be assembled through the Golden Gate assembly method using BsaI restriction enzyme. Golden Gate assembly was selected as our circuit requires the assembly of multiple complex DNA fragments simultaneously [18]. PCR amplification and digestion at the BsaI enzyme sites will be used to isolate the genes of interest [18]. Finally, the destination plasmid will also be digested at the BsaI restriction sites, and the destination vector and inserts will be ligated and yield an assembled plasmid that lacks BsaI restriction sites [19]. The final vector construct will then be ready to be transformed into the host organism. For plasmid 2, The UAS-GAL4 and GFP genes will also be assembled through the golden gate assembly method. Again, PCR amplification and digestion at the BsaI enzyme sites will be used to isolate the inserts and destination vector, and then produce an assembled vector that contains both of the genes of interest [18], [19]. Finally, gel electrophoresis will be performed to make sure that both plasmid 1 and plasmid 2 have been assembled correctly [18].

After the plasmids have been assembled, they must be transformed into the E. coli host cell. However, before transformation can begin, an agar plate containing an ampicillin solution must be created to be used for antibiotic selection. A stock solution of the antibiotic Ampicillin will be created by dissolving the antibiotic powder in water. Addgene's product site recommends making 1000X stock solutions and storing them at -20°C [20]. As pSB1A3 is resistant to the antibiotic Ampicillin [21], the transformation of the plasmid into E. coli will allow the bacteria to express the antibiotic-resistant gene [22]. Placing the bacteria on an agar plate with the antibiotic will kill the bacteria that do not have pSB1A3, allowing only the ones that have the correct plasmid to be able to grow and form colonies.

Competent DNA will be transformed into E. coli cells by undergoing heat shock. E. coli cells are thawed on ice for 10 minutes before transformation occurs [23]. Competent DNA will be added to the thawed E. coli cells and mixed gently [23][8]. Next, this mixture will be placed in a 42°C water bath for 30 seconds [22], [23]. This sudden heat shock that the E. coli cells experience will create a pressure gradient between the extracellular and intracellular space of the E. coli cells, which produces pores in the cell membrane. As a result, the competent DNA will be able to enter the E. coli cells [18]. Next, the E. coli cells will be added to the ampicillin agar plates and incubated overnight while antibiotic selection occurs [23]. Finally, the streaking method will be used to isolate and identify individual colonies of bacteria with those that have survived the antibiotic selection containing the correct backbone [24].

Finally, after the plasmids have been assembled and transformed into the host cell, we will conduct experiments to test the efficacy of our biological circuit. As our circuit outputs GFP in the presence of beta-amyloid oligomers, media with no beta-amyloid present will act as the negative control. On the other hand, our positive control will be media with GAL4-VP16 as that will induce the production of GFP. Our first experiment will be to use fluorescence microscopy to test for the presence of GFP after the host cell has been placed into CSF extracted from an Alzheimer's patient [18], [25]. In our second experiment, we will test the efficacy of our circuit when it is placed in the CSF of a healthy patient by again using fluorescence microscopy to determine GFP output [18], [25]. Overall, these experiments will allow us to demonstrate the efficacy of our biological circuit as it should produce GFP in the presence of beta-amyloid as a diagnostic tool for AD Furthermore, the results from the proposed efficacy experiments will be compared to the results from the Matlab SimBiology program to determine the accuracy of our models.

Results

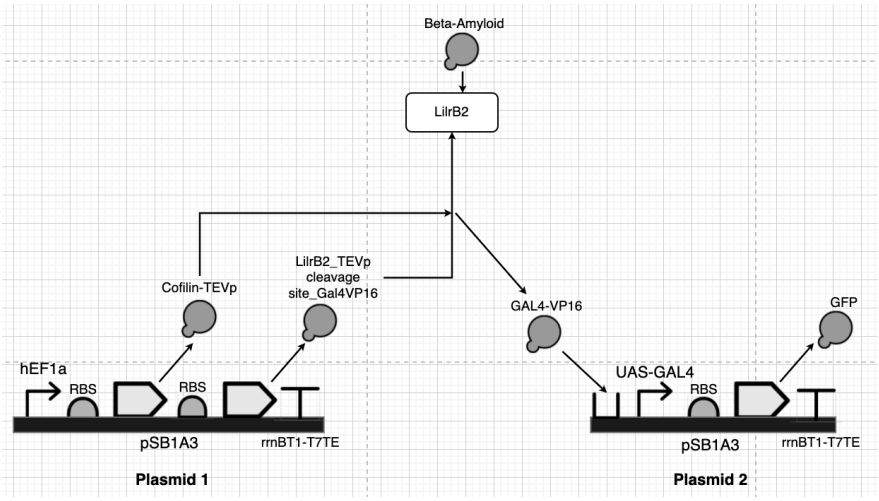

Figure 1: SBOL Schematic of the proposed circuit. Cofilin-TEVp and LilrB2_TEVp cleavage site_GAL4VP16 are constitutively promoted by hEF1a. Once beta-amyloid binds to the LilrB2 receptor, Cofilin-TEVp binds to the TEVp cleavage site and GAL4-VP16 is released. As a result, GAL4-VP16 positively induces the UAS-GAL4 promoter to produce GFP. Overall, the production of GFP should indicate the presence of beta-amyloid in the surrounding environment of the E. coli host.

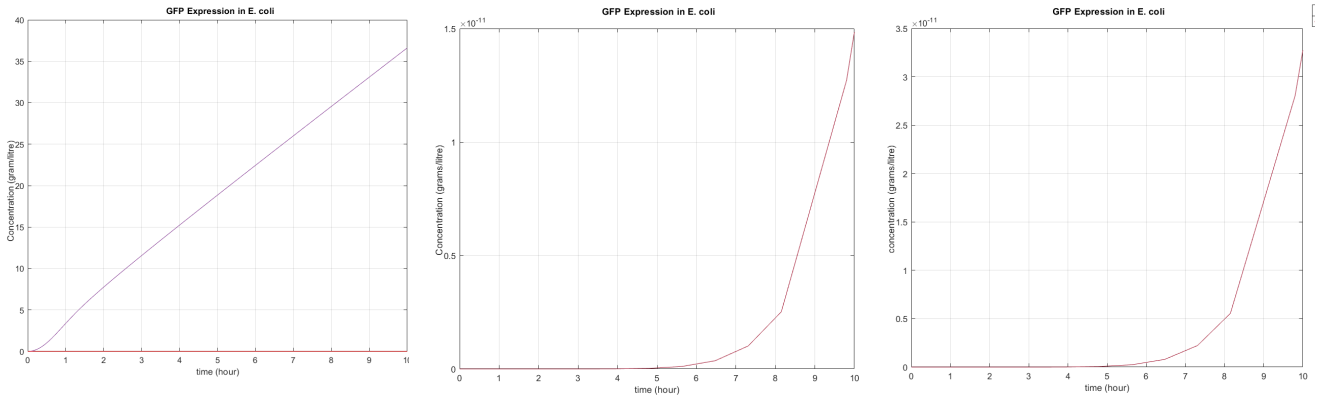

a) Production and expression of Cofilin-TEVp, GAL4 -VP16, the LilrB2-TEVp GAL4-VP16 cleavage site and GFP when beta-amyloid levels are at zero.

b) Expression of GFP when beta-amyloid levels are at 1.13e-6 g/L.

c) Expression of GFP when beta-amyloid levels are at 1.678e-6 g/L.

Figure 2: Production and expression of Cofilin-TEVp (purple), GAL4 -VP16 (red), the LilrB2-TEVp GAL4-VP16 cleavage site (yellow) and GFP (maroon) at varying concentrations of beta-amyloid within E. coli. Larger versions of these graphs can be found in Appendix C.

As shown in Figure 1, the biological circuit produces GFP within E. coli when beta-amyloid is present. This is done through the constitutive production of the Cofilin-TEV protein and LilrB2-TEV protein and GAL4-VP16 cleavage site. Once beta-amyloid (within an external media) binds to the LilrB2 surface receptor on the E. coli it leads to the release of GAL4-VP16 from this complex which induces the UAS-GAL4 promoter to produce GFP. This mechanism can be seen in Figure 2, where the above circuit is placed in media where beta-amyloid levels are at zero (in Figure 2a), at 1.13 e-6 g/L (which is the experimental value of beta-amyloid present in the CSF of AD patients) as shown in Figure 2b, and at 1.678 e-6 g/L (in Figure 2c) [26].

When beta-amyloid levels are at zero (in Figure 2a), GAL4-VP16 is not being released due to a lack of the complexation and cleavage reaction between Cofilin-TEVp and LilrB2-TEVp cleavage site. As a result, it cannot positively induce the UAS-GAL4 promoter to produce GFP. Therefore, both GAL4-VP16 and GFP concentrations remain at zero. This condition serves as a negative control and was conducted to ensure that the circuit is dependent on the presence of beta-amyloid.

Beta-amyloid levels were then increased to 1.13 e-6 g/L (in Figure 2b). At this level, beta-amyloid can bind to the LilrB2 receptor and release UAS-GAL4, positively inducing the UAS-GAL4 promoter to produce GFP. Therefore, when diagnosing a patient - this graph can be used to interpolate and compare the patient's GFP production (through fluorescence microscopy) to a positive control to determine if beta-amyloid levels are lower than basal levels in the CSF.

Finally, in Figure 2c, there is a larger concentration of beta-amyloid. As more beta-amyloid is binding to the LilrB2 receptor, more GAL4-VP16 is being released which results in more GFP being produced. Due to the figures and explanations provided above, we can confirm that GFP indicates the presence of beta-amyloid in the surrounding environment of the E. coli host as expected. The concentration of 1.678 e-6 g/L was used as a control or basal level, as was done by Andreasen et. al., to compare against potential Alzheimer's patients [26].

We made several assumptions for the equations in our biological circuit. The first assumption we made was that the value for the translation efficiency would be the same as the translation efficiency

value used by Elowitz in his article regarding transcriptional regulators [10]. This article uses the steady-state assumption to determine the translation efficiency and mRNA half-lives. The model in the article also uses E. Coli as the host cell, which corresponds to our circuit as well. Due to these similarities, we can assume that the values used in the article are similar to ours. The second assumption was that the association speed (*aps*) and dissociation speed (*dps*) values were assumed to be the same as the *aps* and *dps* values of the CAP and cAMP complexation reaction in an E. coli cell [27]. Due to the specificity of the Cofilin-TEVp and LilrB2-TEVp complexation reaction for our circuit, it was necessary to assume these values to move forward with the modelling. As the CAP and cAMP complexation occur in the same cell type as our model, E. coli [27]. As a result, it is safe to assume the complexation seen in our circuit will have similar values.

Moreover, the graphs represent the expression of GFP in both cases where the CSF of the patient implies AD and does not. Consequently, the results must be interpreted relative to a control test done with the CSF of an individual that does not have AD.

Conclusion

The biological circuit is able to detect the presence of beta-amyloid from a sample of CSF in-vitro. When there was no beta-amyloid present in the sample (Figure 2a), the concentration of GFP remained at zero. As seen in the results, the expression of GFP increases as the concentration of beta-amyloid increases, so we are able to distinguish between a patient with a possible case of AD (Figure 2b) and a healthy individual based on (Figure 2c) CSF levels of the biomarker.

These results indicate that this proposed biological circuit could be used to confirm possible cases of early-stage AD. Next steps will include conducting a study to fine tune the circuit to make sure that the circuit is accurately measuring beta-amyloid concentration, and testing with controls to confirm if the differences in GFP expression are statistically significant. As the tests will take place in-vitro, we could begin human trials and conduct a blind study with individuals that have confirmed cases of possible AD and confirmed healthy individuals in order to check the validity of the simulation results. Testing for a secondary biomarker such as tau will increase the accuracy of this detection method. We recommend that this circuit be used in conjunction with diagnostic imaging to help healthcare providers screen patients for possible cases of AD. Further studies will need to be conducted to address the limitations of this circuit, but this diagnostic tool could be used in the future to allow healthcare providers to detect early signs of AD and patients to begin treatment early.

References

[1] J. Weller and A. Budson, "Current understanding of Alzheimer's disease diagnosis and treatment," *F1000Research*, vol. 7. F1000 Research Ltd, 2018, doi: 10.12688/f1000research.14506.1.

[2] J. Rasmussen and H. Langerman, " Alzheimer's Disease – Why We Need Early Diagnosis ," *Degener. Neurol. Neuromuscul. Dis.*, vol. Volume 9, pp. 123–130, Dec. 2019, doi: 10.2147/dnnd.s228939.

[3] "Alzheimer's Disease Fact Sheet | National Institute on Aging." https://www.nia.nih.gov/health/alzheimers-disease-fact-sheet (accessed Feb. 01, 2021).

[4] S. F. Head E, Powell D, Gold B, "Alzheimer ' s Disease in Down Syndrome," *Eur. J. Neurodegener. Dis.*, vol. 1, no. 3, pp. 353–364, 2014, Accessed: Feb. 01, 2021. [Online]. Available: /pmc/articles/PMC4184282/?report=abstract%0Ahttps://www.ncbi.nlm.nih.gov/pmc/articles/PMC4184282/.

[5] "The Progression of Alzheimer's Disease: What Are the Stages?" https://www.healthline.com/health/stages-progression-alzheimers (accessed Feb. 01, 2021).

[6] M. N. Sabbagh, L. F. Lue, D. Fayard, and J. Shi, "Increasing Precision of Clinical Diagnosis of Alzheimer's Disease Using a Combined Algorithm Incorporating Clinical and Novel Biomarker Data," *Neurology and Therapy*, vol. 6, no. Suppl 1. Springer Healthcare, pp. 83–95, Jul. 01, 2017, doi: 10.1007/s40120-017-0069-5.

[7] A. Perret-Liaudet *et al.*, "Risk of alzheimer's disease biological misdiagnosis linked to cerebrospinal collection tubes," *J. Alzheimer's Dis.*, vol. 31, no. 1, pp. 13–20, 2012, doi: 10.3233/JAD-2012-120361.

[8] A. P. Hrishi and M. Sethuraman, "Cerebrospinal fluid (CSF) analysis and interpretation in neurocritical care for acute neurological conditions," *Indian J. Crit. Care Med.*, vol. 23, no. Suppl 2, pp. S115–S119, 2019, doi: 10.5005/jp-journals-10071-23187.

[9] E. Pedone *et al.*, "A tunable dual-input system for on-demand dynamic gene expression regulation," *Nat. Commun.*, vol. 10, no. 1, pp. 1–13, Dec. 2019, doi: 10.1038/s41467-019-12329-9.

[10] M. B. Elowitz and S. Leibier, "A synthetic oscillatory network of transcriptional regulators," *Nature*, vol. 403, no. 6767, pp. 335–338, Jan. 2000, doi: 10.1038/35002125.

[11] R. Scott McIsaac, B. L. Oakes, D. Botstein, and M. B. Noyes, "Rapid synthesis and screening of chemically activated transcription factors with GFP-based reporters," *J. Vis. Exp.*, vol. 81, no. 81, p. 51153, Nov. 2013, doi: 10.3791/51153.

[12] B. W. Patterson *et al.*, "Age and amyloid effects on human central nervous system amyloid-beta kinetics," *Ann. Neurol.*, vol. 78, no. 3, pp. 439–453, Sep. 2015, doi: 10.1002/ana.24454.

[13] P. Corish and C. Tyler-Smith, "Attenuation of green fluorescent protein half-life in mammalian cells," *Protein Eng. Des. Sel.*, vol. 12, no. 12, pp. 1035–1040, Dec. 1999, doi: 10.1093/protein/12.12.1035.

[14] "Reference Links for Key Numbers in Biology." https://bionumbers.hms.harvard.edu/keynumbers.aspx (accessed Apr. 12, 2021).

[15] "Elowitz2000 - Repressilator | BioModels." https://www.ebi.ac.uk/biomodels/BIOMD0000000012 (accessed Mar. 29, 2021).

[16] A. Sacchetti, T. El Sewedy, A. F. Nasr, and S. Alberti, "Efficient GFP mutations profoundly affect mRNA transcription and translation rates," *FEBS Lett.*, vol. 492, no. 1–2, pp. 151–155, Mar. 2001, doi: 10.1016/S0014-5793(01)02246-3.

[17] "Integrated DNA Technologies | IDT." https://www.idtdna.com/pages (accessed Apr. 12, 2021).

[18] "Team:MIT/Protocols - 2014.igem.org." http://2014.igem.org/Team:MIT/Protocols#GOLDEN_GATE (accessed Apr. 12, 2021).

[19] "Team:MIT/Protocols - 2014.igem.org." http://2014.igem.org/Team:MIT/Protocols#PCR (accessed Apr. 12, 2021).

[20] "Addgene: Molecular Biology Reference." https://www.addgene.org/mol-bio-reference/ (accessed

Apr. 12, 2021).
[21] R. Shetty and T. Knight, “Part:pSB1A3:Get Part - parts.igem.org,” May 04, 2004. http://parts.igem.org/partsdb/get_part.cgi?part=pSB1A3 (accessed Feb. 12, 2021).
[22] “Addgene: Protocol - Bacterial Transformation.” https://www.addgene.org/protocols/bacterial-transformation/ (accessed Apr. 12, 2021).
[23] “INSTRUCTION MANUAL NEB ® Golden Gate Assembly Kit (BsaI-HF ® v2).” Accessed: Apr. 12, 2021. [Online]. Available: www.neb.com/GoldenGate.
[24] “Microbe isolation - Labster Theory.” https://theory.labster.com/microbe-isolation/ (accessed Apr. 12, 2021).
[25] N. K. H. Lim, V. Moestrup, X. Zhang, W. A. Wang, A. Møller, and F. De Huang, “An improved method for collection of cerebrospinal fluid from anesthetized mice,” *J. Vis. Exp.*, vol. 2018, no. 133, Mar. 2018, doi: 10.3791/56774.
[26] N. Andreasen *et al.*, “Cerebrospinal fluid β-amyloid((1-42)) in Alzheimer disease: Differences between early- and late-onset Alzheimer disease and stability during the course of disease,” *Arch. Neurol.*, vol. 56, no. 6, pp. 673–680, Jun. 1999, doi: 10.1001/archneur.56.6.673.
[27] “Elowitz2000 - Repressilator | BioModels.” https://www.ebi.ac.uk/biomodels/BIOMD0000000012 (accessed Apr. 12, 2021).
[28] K. Brandes, “Part:BBa K2100003 - parts.igem.org.” http://parts.igem.org/Part:BBa_K2100003 (accessed Apr. 12, 2021).
[29] J. Anderson, “Part:BBa J61100 - parts.igem.org.” http://parts.igem.org/Part:BBa_J61100 (accessed Feb. 12, 2021).
[30] S. Saha, “Part:BBa K1391115 - parts.igem.org.” http://parts.igem.org/Part:BBa_K1391115 (accessed Apr. 12, 2021).
[31] shinjini Saha, “Part:BBa K1391114 - parts.igem.org.” http://parts.igem.org/Part:BBa_K1391114 (accessed Apr. 12, 2021).
[32] R. Shetty, “Part:BBa B0015 - parts.igem.org.” http://parts.igem.org/Part:BBa_B0015 (accessed Apr. 12, 2021).
[33] “Addgene: pSB1A3-AD011.” https://www.addgene.org/116852/ (accessed Apr. 12, 2021).
[34] “BsaI-HF®v2 | NEB.” https://www.neb.com/products/r3733-bsai-hf-v2#Product Information (accessed Apr. 12, 2021).
[35] “T4 DNA Ligase Buffer (10X).” https://www.thermofisher.com/order/catalog/product/B69?ca&en#/B69?ca&en (accessed Apr. 12, 2021).
[36] “AMPICILLIN Sigma Prod. No. A6140, A9393, and A9518 Storage Temperature 2-8°C.”
[37] G. Robinson, “Part:BBa K511003 - parts.igem.org.” http://parts.igem.org/Part:BBa_K511003 (accessed Apr. 12, 2021).
[38] “Reagents | CODEX-DNA.” https://customer.codexdna.com/shopping/addons/40/ (accessed Apr. 12, 2021).
[39] P. Corish and C. Tyler-Smith, “Attenuation of green fluorescent protein half-life in mammalian cells,” *Protein Eng. Des. Sel.*, vol. 12, no. 12, pp. 1035–1040, Dec. 1999, doi: 10.1093/protein/12.12.1035.
[40] E. Pedone *et al.*, “A tunable dual-input system for on-demand dynamic gene expression regulation,” *Nat. Commun.*, vol. 10, no. 1, pp. 1–13, Dec. 2019, doi: 10.1038/s41467-019-12329-9.
[41] J. H. J. Leveau and S. E. Lindow, “Predictive and interpretive simulation of green fluorescent protein expression in reporter bacteria,” *J. Bacteriol.*, vol. 183, no. 23, pp. 6752–6762, 2001, doi: 10.1128/JB.183.23.6752-6762.2001.
[42] R. Scott McIsaac, B. L. Oakes, D. Botstein, and M. B. Noyes, “Rapid synthesis and screening of chemically activated transcription factors with GFP-based reporters,” *J. Vis. Exp.*, vol. 81, no. 81, p. 51153, Nov. 2013, doi: 10.3791/51153.

Appendix

Appendix A

Table 1: Materials list for the first plasmid (as shown in the SBOL Schematic in Figure 1)

Part	**Name**	**Reference/ iGem number**
promoter	hEF1a (constitutive)	iGem: BBa_k2100003 [28]
RBS		iGem: BBa_J61100 [29]
CDS 1	Cofilin-TEVp	iGem: BBa_K1391115 [30]
CDS 2	LilrB2_TEVp cleavage site_ Gal4VP16	iGem: BBa_K1391114 [31]
Terminator	rrnBT1-T7TE	iGem: BBa_B0015 [32]
Plasmid	pSB1A3	[33]
Enzyme	BsaI	[34]
Buffer	T4 DNA Ligase	[35]
Antibiotic	Ampicillin	[36]

Table 2: Materials list for the second plasmid (as shown in the SBOL Schematic in Figure 1)

Part	**Name**	**Reference Number**
Promoter	UAS-GAL4	iGem: BBa_K511003 [37]
RBS		iGem: BBa_J61100 [29]
Terminator	rrnBT1-T7TE	iGem: BBa_B0015 [32]
Enzymes	T5 Exonuclease Phusion DNA Polymerase Taq DNA Ligase	[38]
Plasmid	pSB1A3	[33]
Buffer	GA1100 Codex DNA's Gibson Assembly HiFi kit	[38]

Appendix B

Table 3: The parameters and their corresponding values and units used to create rate equations for transcription, translation and decay as well as model the biological circuit on Matlab Simbiology.

Parameter	**Value**	**Units**
Translation efficiency [10]	20	proteins/mRNA
Protein half-life [39]	93600	second
mRNA_cofilin_TEVp half-life [10]	120	second
mRNA_LilrB2_TEVp cleavage site_GAL4VP16 half-life [10]	120	second
mRNA_GFP half-life [16]	25200	second
K_tr of hEF1a [40]	73.7	nanomolarity/second
K_tr of UAS-GAL4 [14]	0.94	nanomolarity/second
K [27]	40	molecule/second
average mRNA_cofilin_TEVp lifetime	1	second
average mRNA_LilrB2_TEVp cleavage site_GAL4VP16 lifetime	1	second
average mRNA_GFP lifetime	1	second
k_tl_cofilin_TEVp	1	proteins/mRNA/second
k_tl_LilrB2_TEVp	1	proteins/mRNA/second
k_tl_GFP	1	proteins/mRNA/second
kd_prot	1	1/second
kd_mRNA_cofilin_TEVp	1	1/second
kd_mRNA_LilrB2_TEVp	1	1/second
kd_mRNA_GFP	1	1/second
tps_repr [10]	5.0E-4	transcripts/(promoter*second)
aps [10]	0.4	molecule/second
dps [10]	1.2	1/second
k_assoc	1	molecule/second

k_dissoc	1	1/second
n	1	dimensionless
kf	1	nanomolarity/second
hill_gfp [41]	2	dimensionless
hill_GAL4 [42]	1	dimensionless
Beta-amyloid half-life [12]	9	hour
kd_beta_amyloid	1	1/second

Appendix C

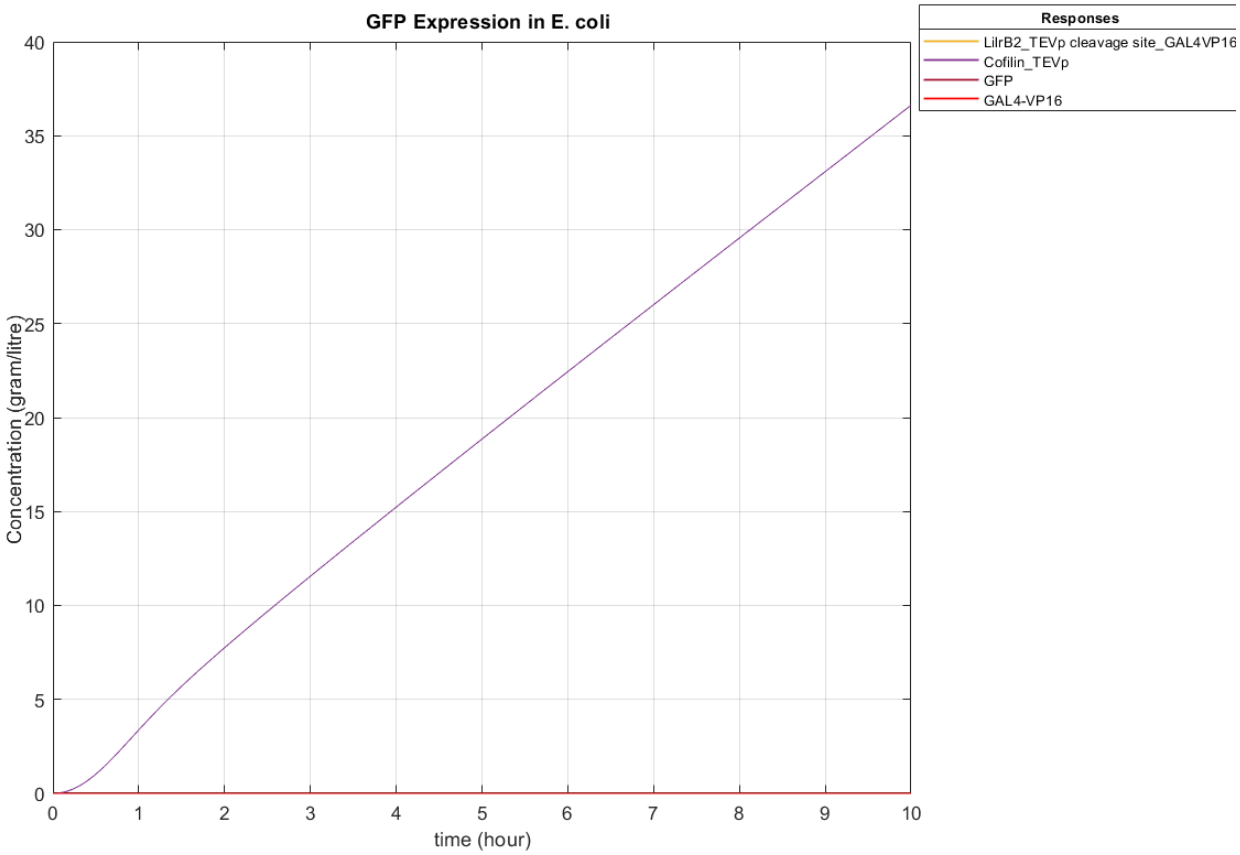

Figure 3: Enlarged version of Figure 2a depicting the production and expression of Cofilin-TEVp, GAL4 -VP16, the LilrB2-TEVp GAL4-VP16 cleavage site and GFP when beta-amyloid levels are at zero.

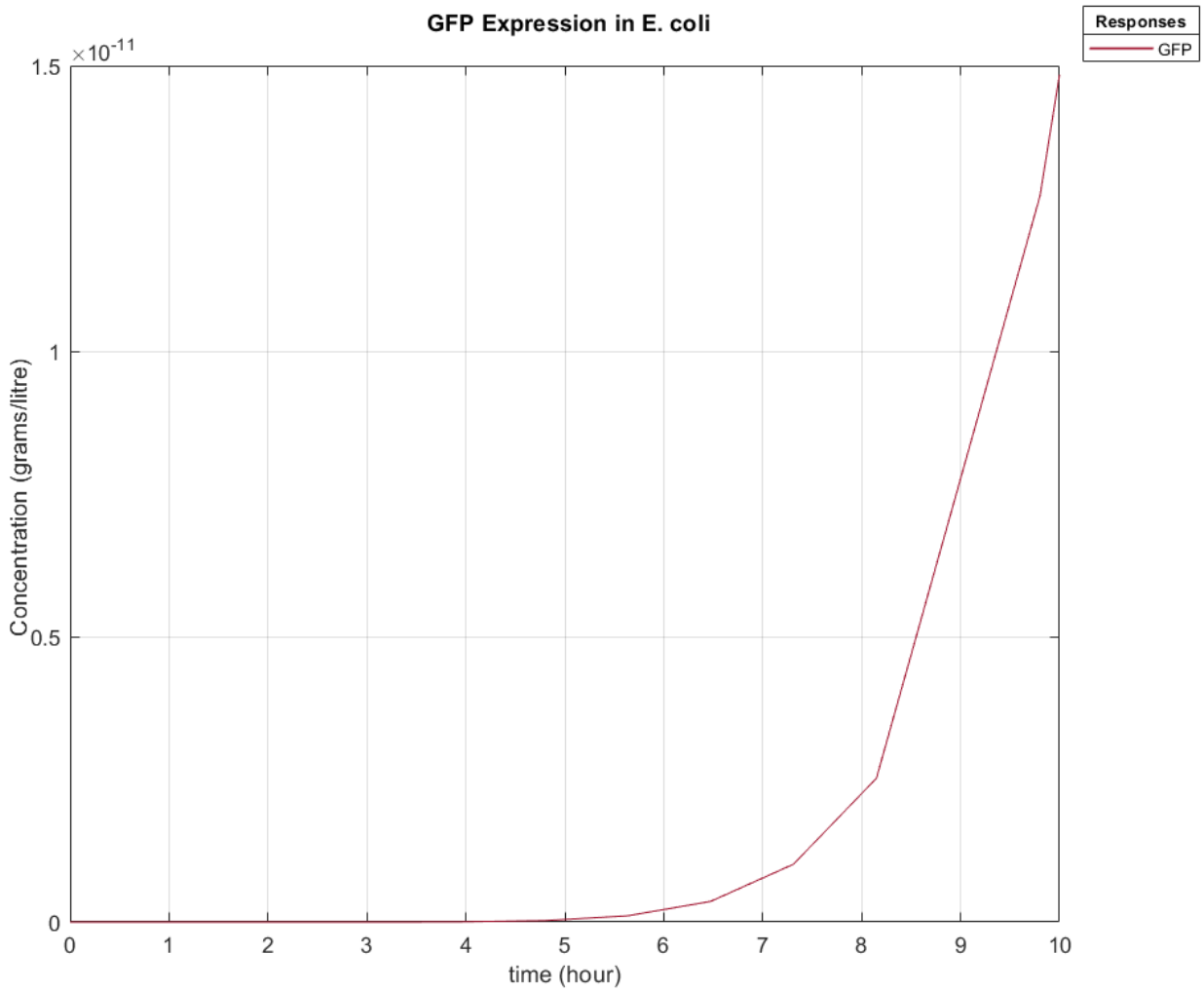

Figure 4: Enlarged version of Figure 2b depicting the expression of GFP when beta-amyloid levels are at 1.13e-6 g/L.

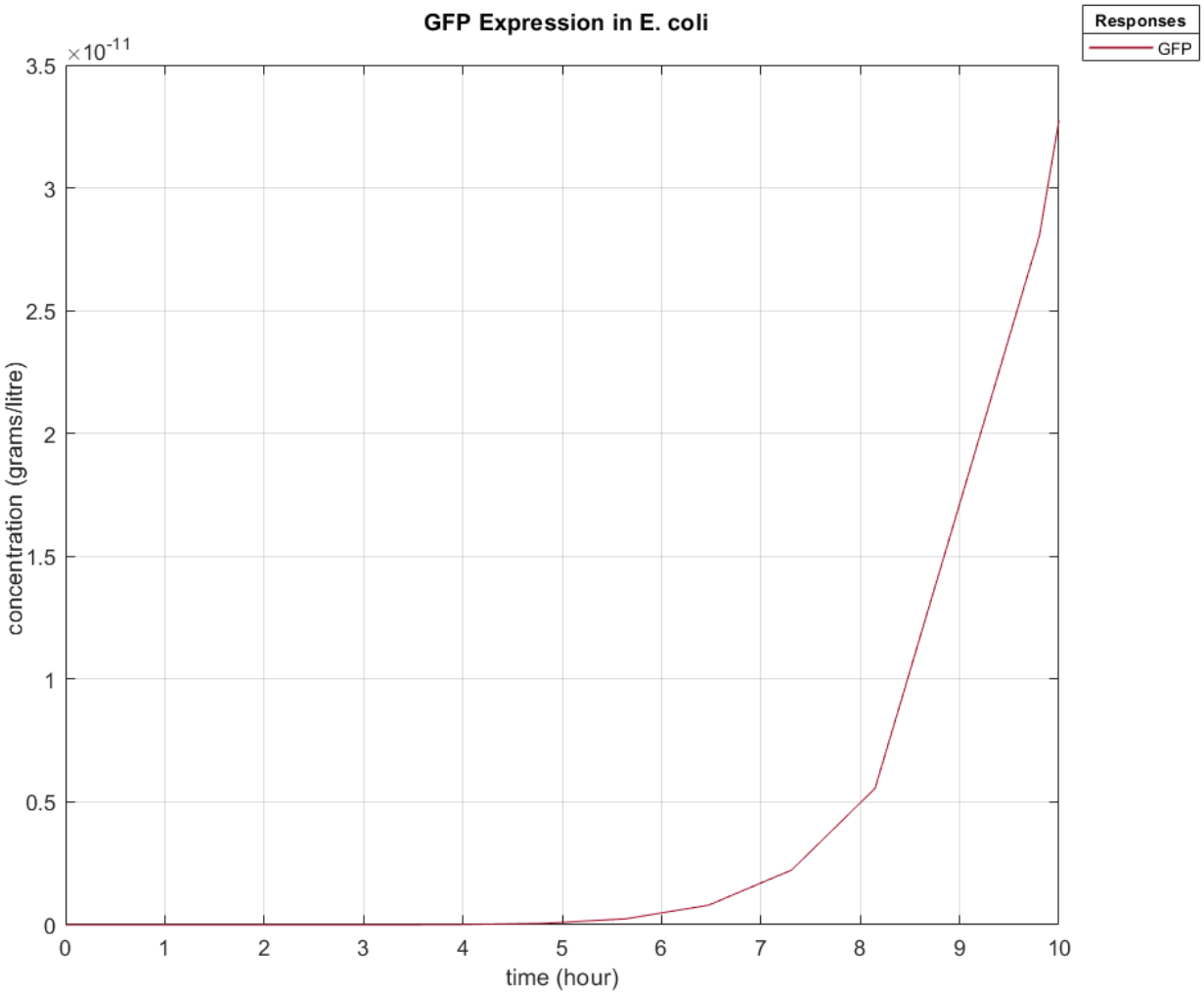

Figure 5: Enlarged version of Figure 2c depicting the expression of GFP when beta-amyloid levels are at 1.678e-6 g/L.

Appendix D

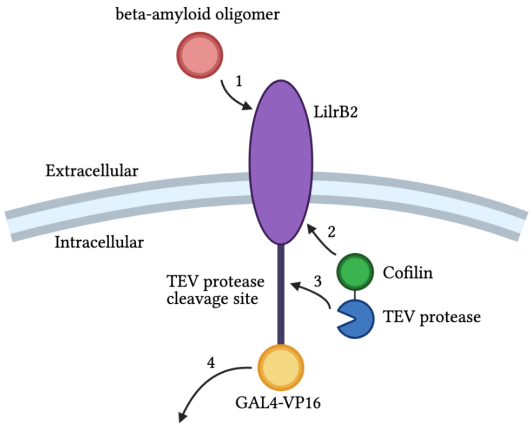

Figure 6: For the Table of Contents only